Ship Detection From Optical Satellite Images Based on Sea Surface Analysis

Guang Yang, Bo Li, Shufan Ji, Feng Gao, and Qizhi Xu

***Abstract*—Automatic ship detection in high-resolution optical satellite images with various sea surfaces is a challenging task. In this letter, we propose a novel detection method based on sea surface analysis to solve this problem. The proposed method first analyzes whether the sea surface is homogeneous or not by using two new features. Then, a novel linear function combining pixel and region characteristics is employed to select ship candidates. Finally, $Compactness$ and $Length\text{-}width\ ratio$ are adopted to remove false alarms. Specifically, based on the sea surface analysis, the proposed method cannot only efficiently block out no-candidate regions to reduce computational time, but also automatically assign weights for candidate selection function to optimize the detection performance. Experimental results on real panchromatic satellite images demonstrate the detection accuracy and computational efficiency of the proposed method.**

***Index Terms*—Sea surface analysis, ship detection, remote sensing.**

I. Introduction

SHIP detection from remote sensing images is essential for traffic monitor, maritime management and illegal fishing surveillance. Synthetic aperture radar (SAR) images are often adopted for ship detection as they are less influenced by weather conditions and time [1]–[3], and they can be utilized to estimate velocities of moving targets [2]. However, SAR images are usually with high-level speckles, insensitive to wood materials, and difficult for human interpretation [4]. Therefore, high-resolution panchromatic satellite images have recently been employed for ship detection, as they can provide more detailed information for small target detection and ship recognition [5]–[9].

Ship candidate selection and false alarm (caused by sea waves, ship wakes, clouds, etc.) elimination are two key issues for ship detection in optical images. Several notable methods have presented in recent literatures. The method in [8] selected ship candidates by morphological filtering, and eliminated false candidates by wavelet analysis and Radon transform. Zhu *et al.* detected ships based on the SVM classifier with shape features and texture features, which could eliminate false alarms to some extent [5], [6]. Proia *et al.* assumed Gaussian distribution of the sea background density function and employed Bayesian decision theory to identify some small-sized ships [7]. Inspired by human visual search, a multiscale and hierarchical method was proposed to detect ships with little computational time [9]. These methods can achieve impressive results due to the powerful ship descriptor and candidate classifier. However, ship appearance is not the only access for ship detection. In fact, the sea surface can provide more important information than the ship appearance.

The complex sea surface usually leads to a major loss and false alarms in ship detection. Therefore, an appropriate sea surface analysis can improve performance of ship detection [10]–[12]. However, the current ship candidate selection methods seldom take the sea surface into consideration. Hence, their performances are easily affected by the variation of illumination and sea surface conditions. In addition, all these methods are implicitly nonlinear, which makes them impractical to be applied in real-time systems. Therefore, we are motivated to present a novel ship detection method based on sea surface analysis (called *SDSSA*). The proposed method can improve the performance of ship detection in terms of the detection accuracy and computational cost.

SDSSA aims to detect the ships that are bigger than 50 pixels in 5m-resolution panchromatic images, with land regions wiped out by geographic information systems. The contribution of this letter is threefold.

First, to the best of our knowledge, we are the first to integrate the sea surface analysis into ship detection in optical images. The sea surface analysis makes *SDSSA* robust to the variation of sea surfaces.

Second, to analyze the sea surface, we define two novel features to describe the intensity distribution of majority and effective pixels. The two features cannot only quickly block out no-candidate regions, but also measure the *I*ntensity *D*iscrimination *D*egree (*IDD*) of the sea surface to assign weights for ship candidate selection function automatically.

Finally, we propose a novel linear ship candidate selection function by using intensity and texture information. Compared with existing methods, *SDSSA* is more efficient in detection accuracy and reducing computational time, thus readily adaptable to real-time processing systems.

The rest of this letter is organized as follows. In Section II, two novel features are defined for sea surface analysis. Our ship detection method is presented in Section III. In Section IV, extensive experiments on real panchromatic satellite images are studied, and we draw conclusions in Section V.

II. Sea Surface Analysis

Sea surfaces show local intensity similarity and local texture similarity in optical images. However, ships and their wakes,

Manuscript received April 8, 2013; revised June 12, 2013 and July 12, 2013; accepted July 13, 2013. Date of publication August 15, 2013; date of current version November 25, 2013. This work was supported in part by the 973 Program (2010CB327900) and the National Science Fund for Distinguished Young Scholars (61125206).

The authors are with the State Key Laboratory of Virtual Reality Technology and System, and Beijing Key Laboratory of Digital Media, School of Computer Science and Engineering, Beihang University, Beijing 100191, China (e-mail: bhboli@vip.sina.com).

Color versions of one or more of the figures in this paper are available online at http://ieeexplore.ieee.org.

Digital Object Identifier 10.1109/LGRS.2013.2273552

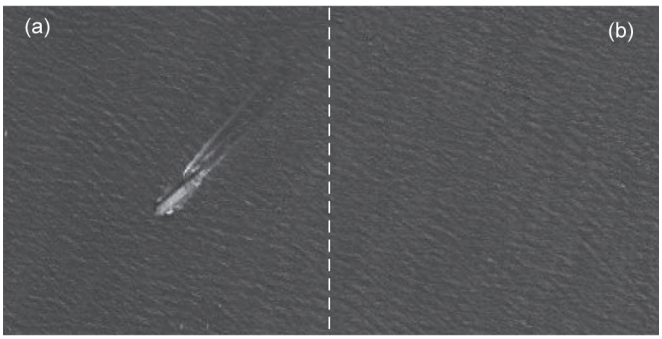

Fig. 1. Sample of sea surface from SPOT 5.

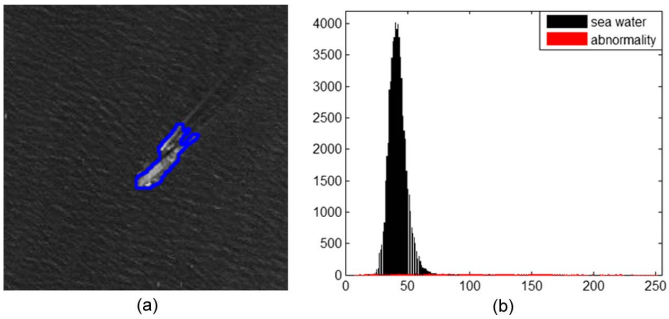

Fig. 2. Different intensity frequencies between water and abnormal regions. (a) The region A of Fig. 1. (b) Intensity frequencies.

as well as clouds and small islands, destroy the aforementioned similarities of sea surfaces. These interference regions become abnormalities as shown in region A of Fig. 1. Hence, ships can be viewed as abnormalities in open oceans and can be detected by analyzing the normal components of sea surfaces.

Sea surfaces are composed of water regions, abnormal regions, and some random noises. As shown in Fig. 2 (the abnormal region of (a) has been labeled with the method proposed in [13]), it is obvious that the main component of the sea surface is sea water, and the effective component is made up of sea water and abnormalities. Moreover, most of intensities of abnormal regions are different from the intensities of sea water, and the intensity frequencies of abnormal regions are much less than that of sea water. Therefore, in order to analyze sea surfaces, two novel features are defined to describe the image intensity distribution on the majority and the effective pixels, respectively.

Since the major region of the image (with land regions wiped out) is self-similar sea water (or large cloud coverage), the intensity frequencies of the majority pixels will be on the top of the descending array of the image grey-level histogram. Thus, we define the *M*ajority *I*ntensity *N*umber as follows:

$$C_m = Min\left\{\arg\left(\sum_{i=1}^{2^b} X(I) > P_1 N_I\right)\right\} \tag{1}$$

where X is the descending array of the image grey-level histogram, b is the digitization bit, P_1 is the percentage which describes the proportion of majority pixels in the image, and N_I is the number of whole image pixels.

C_m can be employed to count the intensity number of P_1 majority pixels. The proportion of random noises in the image is defined as P_2, and the proportion of effective pixels in the image is $1 - P_2$. Thus, we define the *E*ffective *I*ntensity *N*umber as follows:

$$C_e = Min\left\{\arg\left(\sum_{i=1}^{2^b} X(i) > (1 - P_2)N_I\right)\right\}. \tag{2}$$

The number of intensities on the self-similar sea water (or large cloud coverage) is usually smaller than that on complex sea surface with various abnormalities. Moreover, the homogeneous sea surfaces have smaller C_e or C_m values than the heterogeneous ones. For example, $C_m = 23$ and $C_e = 56$ of region A, and $C_m = 24$ and $C_e = 39$ of region B in Fig. 1. Hence, the small value for C_m or C_e can be taken to block out no-candidate regions, which has a relatively low possibilities to contain ships.

Although the intensity distribution difference between ships and waters can help to discriminate ship candidates from various sea surfaces, its effectiveness varies on different kinds of sea surfaces. To measure the effectiveness of intensity discrimination on different sea surfaces, we define another important feature, namely *I*ntensity *D*iscrimination *D*egree (*IDD*), as follows:

$$C_d = C_m / C_e. \tag{3}$$

The larger $C_d (C_d \in (0, 1))$ implies the sea surface is more homogeneous. This means little intensity difference between the majority and the effective pixels, and the intensities of the abnormalities are relatively similar with its backgrounds. Hence, the intensity abnormality on the pixels of the ship is weakened for ship candidate selection. On the contrary, the smaller C_d values imply the intensity abnormality should be emphasized for ship candidate selection.

III. Proposed Ship Detection Method

In this section, we present the workflow of *SDSSA*, which is comprised of three steps. First, the sea surface of the input image is analyzed, and the no-candidate regions are blocked out. Second, the ship candidates are identified by a linear selection function. Third, the ship candidates are further verified to remove false alarms, and to return the detected ships.

A. No-Candidate Region Removal

As mentioned in Section II, small values on C_m and C_e imply less abnormality on pixel intensity, thus the region is of little possibility to contain a ship. Therefore, when $C_m < m$ (or $C_e < e$), the corresponding P_1 (or $1 - P_2$) pixels are blocked out, and only the rest pixels are connected for candidate region selection. The thresholds e and m will be set according to the training data.

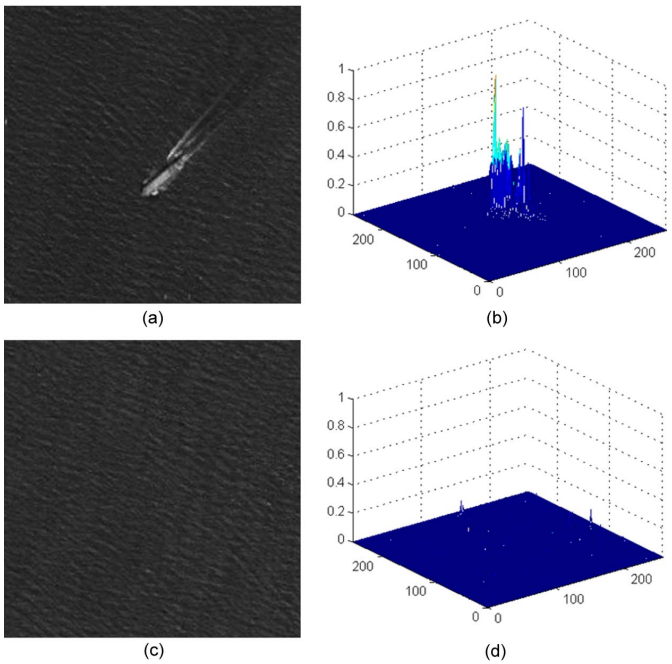

Fig. 3. Examples of ship candidate selection: (a) the region A of Fig. 1; (b) transform result of (a); (c) the region B of Fig. 1; and (d) transform result of (c).

B. Ship Candidate Selection

The intensity abnormality and the texture abnormality are two key features for ship detection. Based on the intensity and the texture features, we propose a novel linear function for ship candidate selection as follows:

$$I'(x,y) = (1 - C_d)/f(x,y) + C_d\sigma_R/m_R \tag{4}$$

where $f(x,y)$ is the intensity frequency of the pixel (x,y). The $f(x,y)$ of the ship is usually very low due to the abnormality and the small size of the ship. Thus, we take $1/f(x,y)$ to emphasize the intensity abnormality of the ship.

As for the texture abnormality, the standard deviation σ is employed to measure the texture roughness of sea surface due to its simplicity and statistical significance. σ is calculated on a region R centered at (x,y). The region has the size of 5×5 pixels and is normalized by the mean intensity frequency m_R. As σ_R/m_R for the edges of the ship is usually high due to the heterogeneous intensities between ships and waters, we employ it to emphasize the texture abnormality of the edges of the ship.

As mentioned in Section II, higher weights should be set to intensity abnormality on sea surfaces with smaller C_d values, where the intensity abnormality is more effective for ship identification. Similarly, the texture abnormality should be higher weighted on sea surfaces with larger C_d values. Therefore, we set $(1 - C_d)$ and C_d as the weight to the intensity and the texture abnormality, respectively.

According to the proposed linear ship candidate selection function, the higher $I'(x,y)$ is, the higher the possibility of ship candidates is. As shown in Fig. 3, the ship candidate can be clearly marked out and the sea water is smoothed on the linear transform result [Fig. 3(b) and (d)]. In the transformed image, the pixels above T_0 are considered as ship candidate pixels. T_0 will be properly set according to the training data.

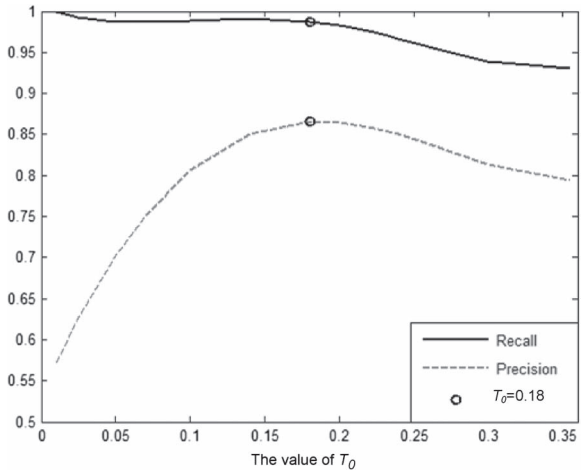

Fig. 4. *Recall* and *Precision* with different values of T_0.

C. False Alarm Elimination

Compactness and *Length-width ratio* have strong discriminative powers to describe the shape of the target. Moreover, the calculation of these two features has a low computing complexity [5]. Therefore, we choose these two features to eliminate false alarms. *Compactness* is taken to describe the shape according to the perimeter $(Perimeter_s)$ and area $(Area_s)$ of candidate regions. *Length-width ratio* is to measure the ratio of the long side $(Long_m)$ to the short side $(Width_m)$ of the minimum bounding rectangle of the region. These two features are defined as follows:

$$Compactness = \frac{(Perimeter_s)^2}{4\pi Area_s} \tag{5}$$

$$Length\text{-}width\ ratio = \frac{Long_m}{Width_m}. \tag{6}$$

After false alarm elimination, the resulting regions are returned as detected ships.

IV. Experimental Results

The proposed method is implemented in C++ with Intel 3.4 GHz CPU. From SPOT-5 and Google Earth service, 159 panchromatic satellite images are collected as testing data set. These images have the size of 9000×9000 pixels with 5m resolution, contain 364 ship targets of different sizes and shapes, and they are captured from various sea surfaces, on different dates and weather conditions.

In order to evaluate the performances of the aforementioned method in different cases, 159 satellite images are subdivided into 9875 subimages with 256×256 pixels size first. And then the subimages are classified into three groups according to the kind of background that they show.

1) Quiet sea: 4281 subimages with no waves, few interferences, and containing 177 ship targets;

TABLE I
DETECTION RESULTS

	Total number of ship targets	Number of detected targets	Number of detected real ship targets	$Recall$	$Precision$	Running Time (min/per image)
Effectiveness of our method in different sea surfaces						
1) quiet sea	177	178	176	99.44%	98.88%	
2) texture sea	150	173	147	98.00%	84.97%	
3) clutter sea	37	48	33	89.19%	68.75%	
Effectiveness of detection phases of our method						
Our method without Step 1	364	399	355	97.53%	88.97%	1.94
Our method without Step 3	364	519	358	98.35%	68.98%	0.98
Our method	364	399	356	97.80%	89.22%	1.19
Comparisons with other detection method						
The method in [7]	364	420	329	90.38%	78.33%	2.85
The method in [8]	364	359	317	87.09%	88.30%	4.23
The method in [9]	364	391	336	92.30%	85.93%	3.79

2) textured sea: 4017 subimages with visible swell or thick cloud cover, and containing 150 ship targets;
3) clutter sea: 1577 subimages with many interferences (scattered clouds, ship wakes, etc.), and containing 37 ship targets.

We employ $Recall$ and $Precision$ to evaluate the performance of *SDSSA*. They are defined as

$$Recall = \frac{\text{Number of detected real ship targets}}{\text{Total number of ship targets of images}} \tag{7}$$

$$Precision = \frac{\text{Number of detected real ship targets}}{\text{Number of detected targets}}. \tag{8}$$

In this section, we first optimize the thresholds of the parameters for *SDSSA* by training data; then we demonstrate the detection effectiveness and the computational cost of *SDSSA*; finally, we give four detection examples of *SDSSA* on extreme cases (e.g., low contrast, strong waves, ship wakes, and cloud coverage).

A. Threshold Optimization

In order to optimize the thresholds of the parameters, 800 subimages with 93 ship targets are carefully chosen as the training data. The training data is comprised of 179 quiet sea subimages, 305 textured sea subimages and 316 clutter sea subimages. In the training experiments, the thresholds are optimized to maximize $Recall$ and $Precision$. As shown in Fig. 4, the $Recall$ and $Precision$ are optimized when the threshold of linear ship candidate selection function is set as $T_0 = 0.18$. And the thresholds of other parameters are set correspondingly: $P_1 = 90\%$, $P_2 = 1\%$, $e = 10$ and $m = 5$. The ranges of $Compactness$ and $Length\text{-}width\ ratio$ are $15 \sim 58$ and $3.5 \sim 16.5$, respectively. In the following experiments, these optimized thresholds are taken for ship detection.

B. Effectiveness of Our Method

In this group of experiments, we first evaluate the performance of our method on different sea surfaces in three subimage groups. As can be seen from Table I, the value of $Precision$ decreases drastically from group 1) to group 3). This means that our method generates false alarms under the interference by clouds, ship wakes, and etc. However, it is noted that the $Precision$ of the proposed method reaches 89.22% for total testing subimages, which indicates that the proposed method is of high accuracy. Especially, *SDSSA* has only eight missed targets and obtains high values of $Recall$ even for clutter sea surfaces. These satisfactory results demonstrate the suitability of the proposed method for automatic ship detection systems.

Second, we assess the capabilities of each part of our method described in Section III. These experiments are carried out on 159 images with 9000×9000 pixels size. As shown in Table I, when we test our method without the step 1 (no-candidate region removal), the average processing time of each image increases by 63% and the value of $Recall$ decreases a little. If we eliminate the step 3 (false alarm elimination) of our detection method, the $Precision$ is dropped dramatically from 89.22% to 68.98%, although the mean running time is reduced and two more ship targets are identified. This means the final step is efficient for moving the false ship candidates following the second step (ship candidate selection). To summarize, the high value of $Recall$ is provided by the second step and the high value of $Precision$ is controlled by the final step, and the first step can reduce computational burden.

Finally, we compare *SDSSA* with the state-of-the-art methods proposed in [4], [5], and [10] on $Recall$, $Precision$ and running time. These experiments are carried out on 159 satellite images with 9000×9000 pixels size. As shown in Table I, our proposed *SDSSA* has better $Recall$, $Precision$ than the methods proposed in [4], [5], and [10]. Moreover, *SDSSA* consumes less average time to process an image, and the 1.19 min processing time for a satellite image with

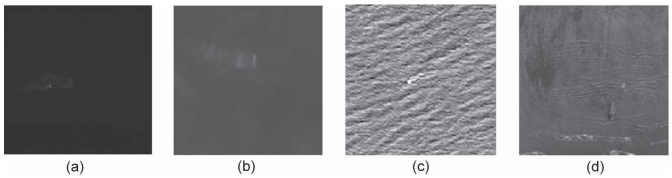

Fig. 5. Examples of extreme cases collected from real panchromatic remote sensing data. (a) Darker ship/low contrast. (b) Cloud coverage. (c) Strong waves. (d) Ship wakes.

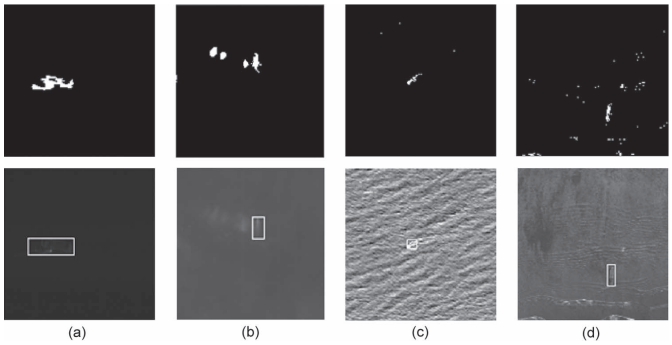

Fig. 6. Detected results of Fig. 5. The first row shows the binary images after ship candidate selection, and the second row presents the detected ships. (a) Darker ship/low contrast. (b) Cloud coverage. (c) Strong waves. (d) Ship wakes.

9000×9000 pixels size makes *SDSSA* suitable for real-time ship detection systems.

C. Performance on Extreme Cases

Several extreme cases exist for ship detection in optical images, which greatly affects the detection performance. Hence, we evaluate *SDSSA* on extreme cases to demonstrate its robustness. Fig. 5 shows some common extreme cases, and the corresponding detected results output by *SDSSA* are shown in Fig. 6, respectively.

Fig. 5(a) provides an example of dark ship on the low contrast sea surface. The lower contrast and dark appearance of the ship increase the difficulty of detection. Nevertheless, *SDSSA* can successfully identify the ship target by assigning higher C_d to intensity abnormality automatically of ship candidate selection function, as shown in Fig. 6(a).

Fig. 5(b) shows an extreme phenomenon that a part of the ship is covered by clouds, whose intensities are similar to the ship. As shown in Fig. 6(b), *SDSSA* can effectively detect the ship hull without cloud pixels. That is because *SDSSA* can automatically set higher weight to the texture feature to emphasize the edge of the ship.

Rough waves are clearly presented in Fig. 5(c), where ship detection is very challenging due to the texture similarity between the edges of the ship and sea waves. As shown in Fig. 6(c), *SDSSA* can successfully identify most of the pixels of the ship with low false rate. It is because that *SDSSA* adaptively increases the weight of intensity abnormality according to the sea surface analysis.

Fig. 5(d) shows a small ship on a complex sea surface with heterogeneous intensity and texture. As demonstrated by Fig. 6(d), many false alarms are extracted after ship candidate selection. Nevertheless, the proposed *SDSSA* can still perform well by utilizing $Compactness$ and $Length\text{-}width\ ratio$. It is clear that *SDSSA* is robust to strong sea clutters.

V. Conclusion

This letter has proposed a novel ship detection method based on sea surface analysis in optical images. To the best of our knowledge, we are the first to integrate sea surface analysis into ship detection in optical images. The proposed method cannot only efficiently block out no-ship regions, but also automatically assign weights to intensity and texture abnormality to optimize detection performance. Compared with existing works, the proposed linear candidate selection function is more computational efficient. The experiments on real panchromatic satellite images demonstrate that *SDSSA* not only outperforms the state-of-the-art methods on $Recall$, $Precision$, and running time, but also is robust to some extreme cases (e.g., dark ships, low contrast, rough waves, ship wakes, and cloud coverage). We believe that the proposed method can have a wide application to the real-time ship detection systems.

References

[1] K. Eldhuset, "An automatic ship and ship wake detection system for space borne SAR images in coastal regions," *IEEE Trans. Geosci. Remote Sens.*, vol. 34, no. 4, pp. 1010–1019, Jul. 1996.

[2] M. V. Dragošvić and P. W. Vachon, "Estimation of ship radial speed by adaptive processing of RADARSAT-1 fine mode data," *IEEE Geosci. Remote Sens. Lett.*, vol. 5, no. 4, pp. 678–682, Oct. 2008.

[3] X. Li and J. Chong, "Processing of envisat alternating polarization data for vessel detection," *IEEE Geosci. Remote Sens. Lett.*, vol. 5, no. 2, pp. 271–275, Apr. 2008.

[4] S. Mirghasemi, H. S. Yazdi, and M. Lotfizad, "A target-based color space for sea target detection," *Appl. Intell.*, vol. 36, no. 4, pp. 960–978, Jun. 2012.

[5] C. Zhu, H. Zhou, R. Wang, and J. Guo, "A novel hierarchical method of ship detection from spaceborne optical image based on shape and texture features," *IEEE Trans. Geosci. Remote Sens.*, vol. 48, no. 9, pp. 3446–3456, Sep. 2010.

[6] G. Jun and Z. Chang-ren, "A novel method of ship detection from spaceborne optical image based on spatial pyramid matching," *Appl. Mech. Mater.*, vol. 190/191, pp. 1099–1103, Jul. 2012.

[7] N. Proia and V. Pagé, "Characterization of a bayesian ship detection method in optical satellite images," *IEEE Geosci. Remote Sens. Lett.*, vol. 7, no. 2, pp. 226–230, Apr. 2010.

[8] C. Corbane, L. Najman, E. Pecoul, L. Demagistri, and M. Petit, "A complete processing chain for ship detection using optical satellite imagery," *Int. J. Remote Sens.*, vol. 31, no. 22, pp. 5837–5854, Jul. 2010.

[9] F. Bi, B. Zhu, L. Gao, and M. Bian, "A visual search inspired computational model for ship detection in optical satellite images," *IEEE Geosci. Remote Sens. Lett.*, vol. 9, no. 4, pp. 749–753, Jul. 2012.

[10] S. Y. Wu and A. K. Liu, "Towards an automated ocean feature detection, extraction and classification scheme for SAR imagery," *Int. J. Remote Sens.*, vol. 24, no. 5, pp. 935–951, Mar. 2003.

[11] Z. Ding, Y. Yu, B. Wang, and L. Zhang, "An approach for visual attention based on biquaternion and its application for ship detection in multispectral imagery," *Neurocomputing*, vol. 76, no. 1, pp. 9–17, Jan. 2011.

[12] F. Totir, E. Radoi, L. Anton, C. Ioana, A. Serbanescu, and S. Stankovic, "Advanced sea clutter models and their usefulness for target detection," *MTA Rev.*, vol. 18, no. 3, pp. 257–272, Sep. 2008.

[13] Q. Xu, B. Li, Z. He, and C. Ma, "Multiscale contour extraction using level set method in optical satellite images," *IEEE Geosci. Remote Sens. Lett.*, vol. 8, no. 5, pp. 854–858, Sep. 2011.